JOURNAL OF BACTERIOLOGY, Apr. 2006, p. 2325–2335 Vol. 188, No. 7
0021-9193/06/$08.00+0 doi:10.1128/JB.188.7.2325–2335.2006

Phenotypic Characterization of *Streptococcus pneumoniae* Biofilm Development

Magee Allegrucci,[1] F. Z. Hu,[2] K. Shen,[2] J. Hayes,[2] Garth D. Ehrlich,[2,3] J. Christopher Post,[2] and Karin Sauer[1]*

Department of Biological Sciences, Binghamton University, Binghamton, New York[1]; Center for Genomic Sciences, Allegheny Singer Research Institute, Pittsburgh, Pennsylvania[2]; and Department of Microbiology and Immunology, Drexel University, College of Medicine, Pittsburgh, Pennsylvania[3]

Received 22 November 2005/Accepted 11 January 2006

***Streptococcus pneumoniae* is among the most common pathogens associated with chronic otitis media with effusion, which has been hypothesized to be a biofilm disease. *S. pneumoniae* has been shown to form biofilms, however, little is known about the developmental process, the architecture, and the changes that occur upon biofilm development. In the current study we made use of a continuous-culture biofilm system to characterize biofilm development of 14 different *S. pneumoniae* strains representing at least 10 unique serotypes. The biofilm development process was found to occur in three distinct stages, including initial attachment, cluster formation, and biofilm maturation. While all 14 pneumococcal strains displayed similar developmental stages, the mature biofilm architecture differed significantly among the serotypes tested. Overall, three biofilm architectural groups were detected based on biomass, biofilm thickness, and cluster size. The biofilm viable cell counts and total protein concentration increased steadily over the course of biofilm development, reaching ~8×10^8 cells and ~15 mg of protein per biofilm after 9 days of biofilm growth. Proteomic analysis confirmed the presence of distinct biofilm developmental stages by the detection of multiple phenotypes over the course of biofilm development. The biofilm development process was found to correlate not only with differential production of proteins but also with a dramatic increase in the number of detectable proteins, indicating that biofilm formation by *S. pneumoniae* may be a far more complex process than previously anticipated. Protein identification revealed that proteins involved in virulence, adhesion, and resistance were more abundant under biofilm growth conditions. A possible role of the identified proteins in biofilm formation is discussed.**

Streptococcus pneumoniae is an important human pathogen that causes an array of diseases, including acute bacterial sinusitis, meningitis, and bacteremia, and remains the major cause of acute bacterial pneumonia and otitis media. Worldwide, approximately 1.1 million deaths annually are attributed to *S. pneumoniae* infection (42). *S. pneumoniae* is among the most common microorganisms isolated from otitis media specimens, others including *Haemophilus influenzae*, *Moraxella catarrhalis*, and *Alliococcus otiditis* (30). The gram-positive, opportunistic pathogen *S. pneumoniae* has been cultured from approximately 40% of middle-ear fluid samples taken from patients with acute otitis media (9, 24).

Next to the common cold, otitis media is the most commonly diagnosed childhood illness in the United States. Otitis media is a clinical diagnosis and the most prevalent infectious disease in children, characterized by the accumulation of fluid in the middle-ear space. Approximately one-third of all children experience three or more episodes of acute otitis media by the age of 3 years (27). Conductive hearing loss is a major consequence of otitis media that may affect the child's behavior, education, or development of language skills (5, 66). The socioeconomic impact of otitis media is staggering, with annual costs exceeding $5 billion in the United States alone (38).

Recent findings support the hypothesis that biofilms play a major etiologic role in otitis media and its frequent complications, including posttympanostomy otorrhea (24). Biofilms are complex, organized communities of bacteria that grow in association with a wide array of biotic and abiotic surfaces (15, 17, 25). Biofilm growth can occur at almost any solid-liquid interface in industrial and clinical settings (14, 29, 39–40). Biofilms are inherently resistant to antimicrobial agents and are often the root cause of persistent implant- and non-implant-related bacterial infections and diseases such as cystic fibrosis, urinary tract infections, and periodontitis (16, 43, 61).

Scanning electron micrographs of the middle ear mucosa of a chinchilla have in part elucidated the contribution of biofilms to the pathogenesis of chronic otitis media with effusion. The presence of microcolonies 1 day and 21 days postinoculation of all middle-ear specimens suggests biofilm involvement during the disease state (24). Although biofilm formation by *S. pneumoniae* has been suggested in individuals who develop otitis media (22, 24), the majority of studies have focused on the pathogenic nature of *S. pneumoniae* independent of its ability to form biofilms.

Three notable exceptions depict biofilm formation by *S. pneumoniae*. Budhani and Strutters (13) used a continuous-culture system (sorbarod filter) to determine antimicrobial susceptibilities of *S. pneumoniae* biofilms, while Waite et al. (70) employed the same continuous-culture biofilm system to investigate variation in capsule production upon biofilm formation by serotype 3 pneumococci. Likewise, Donlan et al. (23) used a continuous-culture model system allowing the simultaneous measurement of cells and exopolysaccharide of biofilm-associated *S. pneumoniae* in situ over time.

* Corresponding author. Mailing address: State University of New York at Binghamton, Department of Biological Sciences, 104 Science III, Vestal Parkway East, Binghamton, NY 13902. Phone: (607) 777-3157. Fax: (607) 777-6521. E-mail: ksauer@binghamton.edu.

TABLE 1. *Streptococcus pneumoniae* strains and clinical isolates used in this study

Strain	Capsule serotype	Origin of clinical isolates[a]	Source
ATCC 6303	3	NA	ATCC
BS68	9	NP swabs/nose	D. Greenberg[b]
BS69	14	NP swabs/nose	D. Greenberg
BS70	11	NP swabs/nose	D. Greenberg
BS71	3	NP swabs/nose	D. Greenberg
BS72	23	NP swabs/nose	D. Greenberg
BS73	6	NP swabs/nose	D. Greenberg
BS74	18	NP swabs/nose	D. Greenberg
BS75	19	NP swabs/nose	D. Greenberg
CHPA	ND	External ear	D. Greenberg
CHPB	ND	External ear	D. Greenberg
CHPC	ND	External ear	D. Greenberg
38	W2938	Sputum	D. Greenberg
44	F3114	ND	D. Greenberg

[a] NA, not applicable; ND, not determined; NP, nasopheryngeal.
[b] Children's Hospital of Pittsburgh.

While these studies demonstrate the biofilm formation ability of *S. pneumoniae*, the studies are narrow with respect to analysis of a single clinical isolate or specific capsule serotype. Furthermore, none of the biofilm culture systems used in the studies described above generated sufficient biomass for more detailed phenotypic characterizations of pneumococcal biofilm development by proteomic approaches. While it is now widely accepted that microorganisms undergo profound changes during their transition from planktonic (free-swimming) organisms to cells that are part of a complex, surface-attached community (55–56, 65), information is lacking as to whether biofilm formation in *S. pneumoniae* correlates with profound phenotypic changes at the gene and protein level.

Here, we describe a biofilm culture system that is suitable not only for growing various *S. pneumoniae* capsule serotypes but also for defining the transitional stages of *S. pneumoniae* biofilm development. Furthermore, we provide evidence that *S. pneumoniae* displays multiple phenotypes over the course of biofilm development.

MATERIALS AND METHODS

Bacterial strains and media. All strains used in this study are listed in Table 1. Eight pneumococcal strains, designated BS68 to BS75, were obtained as nasal washes from symptomatic pediatric participants at Children's Hospital of Pittsburgh who were enrolled in a pneumococcal vaccine trial (60). Three additional pneumococcal strains were obtained from the middle ear and one from sputum. The strains were a gift from David Greenberg. The reference strain ATCC 6303 was obtained from the American Type Culture Collection (ATCC).

Growth conditions. All strains listed in Table 1 were subcultured from a frozen stock on Trypticase soy agar (TSA II) supplemented with 5% sheep's blood (Becton Dickinson, Sparks, MD) at 37°C in 5% CO_2. A single colony was used to inoculate 20 ml of Todd-Hewitt broth (Acumedia, Neogen Corporation; Lansing, MI), which was then incubated for 12 h at 37°C in 5% CO_2. The overnight culture was then used to inoculate 50 ml of fresh Todd-Hewitt broth. The culture was grown to mid-logarithmic phase (turbidity of ~0.5 at 600 nm) and used to inoculate the biofilm reactor as described below. The viable cell counts (~8.4×10^7 CFU/ml) were determined by serial dilution and plating on blood agar followed by incubation at 37°C in a CO_2 incubator.

Biofilm formation using flow cells. A continuous-culture once-through flow cell previously described (55, 57) was configured to observe the growth and development of *S. pneumoniae* biofilms attached to a glass substratum. Diluted (0.2-fold) Todd Hewitt medium (6 g/liter) was used as a growth medium. The flow cell was constructed of anodized aluminum containing a chamber (4.0 mm by 1.3 cm by 5.0 cm) having two glass surfaces, one being a microscope slide and the other being a glass coverslip serving as the substratum. Briefly, *S. pneumoniae* cells grown to mid-exponential phase (4 ml) served as the inoculum and were injected into a septum 4 cm upstream from the flow cell. Bacteria were allowed to attach to the glass substratum for 2 h prior to initiating flow. The flow rate of the system was adjusted to 0.014 ml/min. Flow through the chamber was laminar, with a Reynolds number of <0.5, having a fluid residence time of 180 min. Biofilms were grown for up to 9 days under flowing conditions at 37°C in 5% CO_2. Biofilms were then visualized over time, by either bright-field microscopy or confocal laser scanning microscopy (CLSM) as described below.

Microscopy and image acquisition. Cells attached to the inner surface of the glass coverslip were viewed by transmitted light using an Olympus BX60 microscope (Olympus, Melville, NY) and a 1,000× magnification A100PL objective lens. Images were captured using a Magnafire cooled three-chip charge-coupled device camera (Optronics Inc., Galena, CA) with 30-ms exposure. In addition, confocal scanning laser microscopy was performed with an LSM 510 Meta inverted microscope (Zeiss, Heidelberg, Germany). Images were obtained with an LD-Apochrome 40×/0.6 lens and the LSM 510 Meta image acquisition software (Zeiss). To visualize the biofilm architecture of 6- and 9-day-old biofilms, biofilms were stained using the Live/Dead BacLight stain from Invitrogen (Carlsbad, CA). Quantitative analysis of epifluorescence microscopic images obtained from flow cell-grown biofilms at the 6-day time point was performed with COMSTAT image analysis software (35).

Biofilm formation using a continuous-flow tube reactor. Biofilms were grown as previously described (55, 57) for protein sampling with the following exceptions. Biofilms were grown on the interior surfaces of 1-m-long, size 16 Masterflex silicone tubing (total interior volume, 6.0 ml; total surface area, 150 cm^2; Cole Parmer Inc.) of a once-through continuous-flow tube reactor system. Diluted (0.2-fold) Todd-Hewitt medium (6 g/liter) was used as a growth medium. The biofilm reactor was inoculated with 6 ml of a planktonic *S. pneumoniae* suspension as described above. The flow rate of the system was adjusted to 0.035 ml/min with a retention time of approximately 180 min. Following inoculation, the flow was stopped for 2 h to allow attachment. Biofilms were grown for 3, 6, and 9 days under flowing conditions at 37°C in 5% CO_2. Biofilm cells were harvested from the interior surface by pinching the tube along its entire length, resulting in extrusion of the cell material from the lumen. The resulting cell paste was collected on ice. Prior to sampling, the bulk liquid was purged from the tubing to prevent interference from detached, planktonic cells.

Preparation of crude protein extracts and protein determination. Batch- and biofilm-grown *S. pneumoniae* cells were immediately washed after sampling by centrifugation at 12,000 × *g* for 10 min at 4°C and resuspended in TE buffer (10 mM Tris-HCl, 1 mM EDTA, pH 8.0), containing 0.3 mg phenylmethylsulfonyl fluoride/ml (Boehringer Mannheim, Indianapolis, IN). All cell samples were lysed by sonication on ice using six 10-second bursts at 5 W (Cole Parmer Instrument Co., Vernon Hills, IL) and stored at −20°C. Cell debris and unbroken cells were removed from all samples by centrifugation at 16,000 × *g* for 5 min at 4°C. Total protein concentration was determined by a modified method (51) using reagents from Sigma. Bovine serum albumin was used as the standard. Experiments for each time point were performed in triplicate.

Correlation of protein concentration and CFU over the course of *Streptococcus pneumoniae* biofilm development. The number of viable cells in both planktonic and biofilm cultures was determined by the number of CFU using serial dilution plate counts (63). To do so, biofilms were harvested from the interior surface as described above, with the resulting cell pastes resuspended in saline (total volume, 1 ml) and homogenized for 30 seconds to disrupt cell clusters. Bacterial cells were grown on blood agar plates at 37°C in 5% CO_2 overnight. The protein concentration was determined in parallel as described above. Planktonic cells were harvested in logarithmic phase. Experiments for each time point were performed in triplicate.

Two-dimensional (2D) gel electrophoresis and image analysis. The protein production patterns of total cell extracts of planktonic and biofilm cells were analyzed by 2D polyacrylamide gel electrophoresis (PAGE) as described previously (54–55) with the following exceptions: Proteins were separated in the first dimension using 18-cm-long Immobiline Dry Strips having a pH gradient of 3 to 10 (nonlinear), 4 to 7, and 4.5 to 5.5 (GE Healthcare, Piscataway, NJ). The Immobiline Dry Strips were focused for a total of 48.0, 65.0, and 70.5 kVh, respectively. The 2D gels were stained with silver nitrate (10) and run in triplicate for each growth condition to confirm the reproducibility of the protein patterns under planktonic and biofilm growth conditions. A calibrated image scanner (GE Healthcare) was used for gel scanning to ensure even spot detection and higher accuracy for the subsequent image analysis. Computational image analysis was carried out using Image Master 2D Platinum software (GE Healthcare).

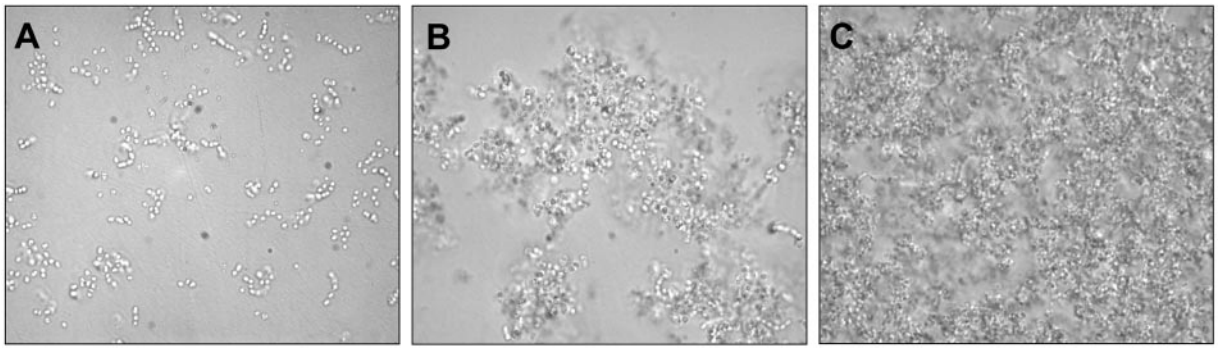

FIG. 1. *Streptococcus pneumoniae* biofilm formation under continuous flow. Phase-contrast micrographs at a magnification of 1,000× obtained 1 day (A), 2 days (B), and 3 days (C) after initiation of *S. pneumoniae* biofilm formation. Biofilms were viewed using an Olympus BX60 microscope. Flow-cell experiments were performed in triplicate as described in Materials and Methods.

Protein identification by mass spectrometry. Protein spots of interest were excised from the gel and digested in situ with trypsin using a ProGest workstation (Genomics Solutions Inc., MI). After digestion for 6 h at 37°C, tryptic peptides were extracted and desalted if necessary using ZipTips (Millipore). An aliquot of the supernatant was taken for analysis by matrix-assisted laser desorption ionization-time of flight (MALDI-TOF) mass spectrometry using an Ettan MALDI-TOF Pro (GE Healthcare, Piscataway, NJ) as described previously (57, 63). Trypsin peptides were used as internal standards for every peptide sample to ensure high mass accuracy. The peptide mass fingerprinting spectra were processed using the Ettan Evaluation software (GE Healthcare) and the mass lists generated were subsequently used for database searches using the ProFound search algorithm (73).

The database used in this study was composed of protein sequences obtained from TIGR (comprehensive microbial resource batch download website, http://www.tigr.org/tigr-scripts/CMR2/batch_download.dbi) and comprised the sequences of *S. pneumoniae* R6, *S. pneumoniae* TIGR4, *Streptococcus pyogenes* M1, *Staphylococcus aureus* MRSA252, *Staphylococcus epidermidis*, *Enterococcus faecalis* V583, *Escherichia coli* K12-MG1655, *and Pseudomonas aeruginosa* PAO1. All proteins were identified with significant certainty (probability score of <0.03). Proteins were identified with 3 to 15 matched peptides and a minimum of 5% sequence coverage.

RESULTS

To characterize the biofilm developmental life cycle of *Streptococcus pneumoniae*, we made use of a once-through biofilm reactor system (55, 57, 63) modified to accommodate the growth characteristics of *S. pneumoniae*. In particular, biofilms were grown at 37°C in 5% CO_2 under flow conditions in reactors having a fluid residence time of 180 min. Shorter residence times resulted in a decrease in the biofilm biomass over time (data not shown). For this reason, diluted Todd-Hewitt medium was used. The growth conditions were optimized using the *S. pneumoniae* serotype 3 clinical isolate (BS71) and the reference strain (ATCC 6303, serotype 3).

Biofilm development in *Streptococcus pneumoniae* serotype 3 occurs in stages. Bright-field microscopy enabled the direct observation of distinct stages of *S. pneumoniae* biofilm development, from initial attachment to the appearance of small complex clusters on the substratum. As shown in Fig. 1, diplococci as well as chains of cells were visible on the glass substratum within 1 day of inoculation (Fig. 1A). By day 2, small clusters of cells exceeding 20 μm in width and height were detectable (Fig. 1B). Three days postinoculation, the biofilm appeared more structurally complex with the entire surface of the substratum covered with cells interspersed with larger cell clusters (Fig. 1C). To further visualize the three-dimensional architecture of *S. pneumoniae* biofilms, confocal laser scanning microscopy was used to image 6- and 9-day-old biofilms. The confocal images depicted in Fig. 2A and B correspond to 6- and 9-day-old biofilms, respectively. Both images reflect biofilm structures comprised of large cell clusters exceeding 80 μm in width and 100 μm in height. Also indicative of a mature biofilm was the presence of intervening water channels (Fig. 2).

Overall, biofilm formation in *S. pneumoniae* serotype 3 strains occurred in a sequential process of initial attachment of individual cells to a surface, formation of cell aggregates, and further cell proliferation and biofilm maturation.

Biofilm development in *Streptococcus pneumoniae* correlated with an increase in CFU and biomass. *S. pneumoniae* has been reported to lyse during stationary phase when grown under batch conditions in liquid (4). Biofilms grown under continuous flow have been shown to undergo conditions such as stagnation, similar to that of stationary phase. We were therefore interested in whether the use of a continuous-flow biofilm tube reactor system allowed biofilms to be sustained for 9 days without significant lysis.

To do so, the number of viable cells was correlated to the total protein concentration obtained from biofilm cells after 3, 6, and 9 days of biofilm growth. The results are shown in Table 2.

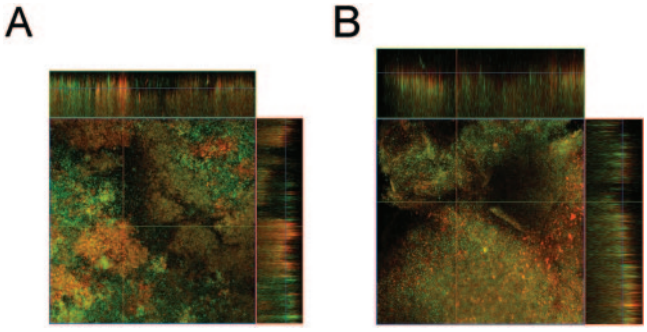

FIG. 2. Confocal laser scanning microscopic images of (A) 6-day and (B) 9-day-old *Streptococcus pneumoniae* serotype 3 biofilms. Biofilms were grown in flow cells under once-through flow conditions for 6 and 9 days, after which time the biofilms were stained with the Live/Dead BacLight stain. Biofilms were viewed at 400× magnification. Flow cell experiments were performed in triplicate as described in Materials and Methods.

TABLE 2. Viable counts and total protein concentration of *Streptococcus pneumoniae* biofilms collected from once-through biofilm tube reactors[a]

Biofilm age (days)	Viable cell count per biofilm[b] (CFU)	Total protein concentration per biofilm[b] (μg)
3	1.96×10^8 (3.9×10^7)	1,968 (560)
6	3.87×10^8 (1.1×10^7)	6,897 (2,210)
9	6.74×10^8 (1.1×10^7)	14,950 (2,192)

[a] CFU and protein concentration were obtained from 3-, 6-, and 9-day-old biofilms. Numbers in parentheses are standard deviations.
[b] The total surface area per biofilm was 150 cm^2.

Approximately 2×10^8 viable cells colonized one biofilm tube within the first 3 days, and the viable cell counts increased upon continued incubation in the biofilm tube reactor to approximately 7×10^8 after 9 days of biofilm growth (Table 2). In parallel, the protein concentration was shown to increase over time (Table 2). The ratio of viable cells to the protein yield over the course of biofilm development was observed to be constant, with 10^8 cells yielding 1 μg of protein ($y = 36705x + 1.0 \times 10^8$, $R^2 = 0.9995$). This finding indicated that the biofilm growth conditions used in this study not only prevented cell lysis but also allowed continued biofilm growth for 9 days. This was achieved by inoculating the biofilm reactor with a log-phase culture and maintaining batch conditions for only 2 h prior to pumping fresh medium into the reactor.

Characterization of biofilm architecture of *Streptococcus pneumoniae* clinical isolates. *S. pneumoniae* is characterized by extensive interstrain phenotypic and genotypic diversity as demonstrated by the ability of different isolates to produce 90 serologically distinct types of capsular polysaccharide (33, 45) and the finding that each strain varies in genomic content from every other strain by 5 to 10% (60). To determine whether the biofilm growth conditions were suitable for various other *S. pneumoniae* serotypes and/or clinical isolates, we analyzed the three-dimensional structure of biofilms of various *S. pneumoniae* clinical isolates (see Table 1) by CLSM after 6 days of biofilm growth.

Under the conditions used, all clinical isolates tested in this study (see Table 1) were able to form biofilms. However, the biofilms formed by the clinical isolates differed with respect to their mature biofilm architecture, especially with regard to the size of the microcolonies, overall biomass, and biofilm height. Visually, three types of biofilm architecture were discernible. Their overall architecture is shown in Fig. 3. Group I consisted of highly structured biofilms composed of large, distinct microcolonies and pronounced water channels (Fig. 3A). The average cluster size ranged from 40 to 150 μm in diameter and the biofilm height ranged from 90 to 150 μm. This type of architecture was found for *S. pneumoniae* strains ATCC 6303, BS71, BS72, and CHPB. Group II was comprised of biofilms formed by *S. pneumoniae* strains BS68, BS69, BS70, BS73, and BS74. These biofilms appeared to be less structured, lacking the large, distinct mound-shaped microcolonies and pronounced water channels seen for group I (Fig. 3B). However, smaller microcolonies and clusters were observed with biofilm heights comparable to that of group I biofilms. Group III biofilms were produced by strains CHPA, CHPC, F3114, W2938, and BS75 and exhibited a flatter structure containing less biomass (Fig. 3C) than groups I and II. The group III biofilms appeared more granular due to the presence of very small cell clusters (<20 μm) and dispersed small microcolonies not exceeding 20 μm in diameter.

The differences in biofilm architecture among the three groups are most likely not attributable to differences in growth rates. In fact, the doubling times were similar among the different strains (~60 min) with the exception of strains BS70 and CHPA (120 min). The biofilms formed by these two strains were categorized as groups II and III, respectively.

Quantitative analysis of biofilm architecture of *Streptococcus pneumoniae* clinical isolates. Visual inspection of the various biofilm structures formed by the different *S. pneumoniae* strains led to their classification into one of three distinct groups. To

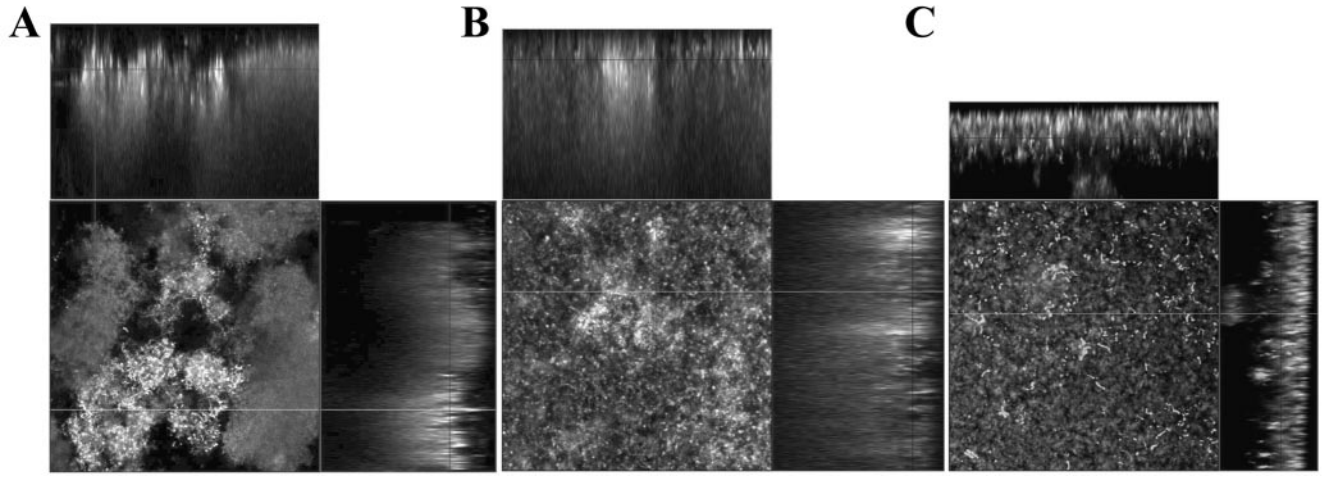

FIG. 3. Confocal laser scanning microscopic images of 6-day-old biofilms of *Streptococcus pneumoniae* serotypes. Representative CLSM images of *S. pneumoniae* group I biofilm architecture (A) of strain BS71 (serotype 3), group II biofilm architecture (B) of strain BS73 (serotype 6), and group III biofilm architecture (C) of strain BS75 (serotype 19) are shown. Biofilms were grown in flow cells under once-through flow conditions for 6 days, after which time the biofilms were stained with the Live/Dead BacLight stain. Biofilms were viewed at 400× magnification. The CLSM images show the *xy* and *xz* planes. Flow cell experiments were performed in triplicate as described in Materials and Methods.

TABLE 3. Quantitative analysis of biofilm structure[a] formed by various *Streptococcus pneumoniae* capsule serotypes

Biofilm architecture group	Strain and serotype	Biomass ($\mu m^3/\mu m^2$)	Avg thickness (μm)	Maximum thickness (μm)	Substratum coverage	Roughness coefficient
I	Type 3	121.57 (4.9)	139.92 (9.7)	150.98 (6.4)	0.403 (0.08)	0.118 (0.09)
	CHPB	109.14 (6.3)	103.70 (1.5)	104.87 (2.2)	0.471 (0.1)	0.016 (0.005)
	Type 23	80.48 (0.04)	100.76 (3.3)	146.03 (3.5)	0.050 (0.01)	0.326 (0.01)
	ATCC (type 3)	78.96 (2.2)	88.54 (4.8)	89.88 (5.2)	0.259 (0.03)	0.021 (0.006)
II	Type 18	64.20 (3.4)	69.72 (4.6)	81.46 (2.7)	0.185 (0.03)	0.083 (0.002)
	Type 6	64.07 (0.7)	65.10 (1.7)	65.58 (2.1)	0.158 (0.04)	0.023 (0.005)
	Type 9	58.00 (6.4)	60.47 (6.5)	72.09 (10.5)	0.129 (0.04)	0.110 (0.01)
	Type 11	54.59 (6.6)	60.23 (9.3)	64.82 (11.0)	0.026 (0.008)	0.088 (0.02)
	Type 14	44.90 (9.6)	56.83 (14.2)	110.55 (14.7)	0.124 (0.08)	0.331 (0.06)
III	CHPA	36.16 (3.9)	39.40 (4.1)	57.00 (10.3)	0.060 (0.03)	0.156 (0.03)
	F3114	35.10 (2.3)	47.75 (6.4)	74.00 (2.8)	0.031 (0.03)	0.472 (0.02)
	Type 19	31.26 (5.3)	36.70 (5.3)	62.66 (4.4)	0.041 (0.03)	0.154 (0.01)
	W2938	27.49 (22.2)	38.38 (24.1)	77.50 (20.5)	0.051 (0.03)	0.526 (0.1)
	CHPC	21.29 (5.3)	29.58 (2.5)	105.30 (2.5)	0.036 (0.04)	0.897 (0.1)

[a] Values are means of data from six *z* series image stacks for each strain or serotype taken at day 6. The numbers in parentheses are the standard deviations.

confirm these observations, we utilized the COMSTAT image analysis program. As shown in Table 3, five variables were used to evaluate biofilm architecture. The major difference between the three biofilm architectural groups was total biomass. Group I consisted of biofilms with biomass exceeding 75 $\mu m^3/\mu m^2$. The biomass of group II biofilms ranged between 40 and 70 $\mu m^3/\mu m^2$ while group III biofilm biomasses were consistently below 40 $\mu m^3/\mu m^2$.

The primary distinguishing characteristic of group I compared with group II was a greater biomass and higher average and maximum thickness. The decreased total biomass of the group II biofilms compared to group I was consistent with the lack of large, distinct microcolonies (Fig. 3). The substratum coverage for all representatives of group I and II is between 0.25 and 0.45, with a roughness of ~0.02 to 0.11. The only exception in group I is BS72 (type 23), with a substratum coverage of 0.05 and a roughness of ~0.3. In group II, BS69 (type 14) showed a higher roughness than the other representatives of this group. Group III biofilms were characterized by an average biomass of <40 μm and an average thickness of ~40 μm. Furthermore, the increase in roughness within group III compared to group I and II biofilms is indicative of the overall appearance of flat, unstructured biofilms lacking pronounced water channels. Taken together, these quantitative analyses support our visual observations of the biofilm architecture formed by the *S. pneumoniae* strains (Fig. 3, Table 3).

Proteomic analysis of biofilm development in *Streptococcus pneumoniae*. Our findings indicated that the biofilm developmental process exhibited by *S. pneumoniae* occurred in stages (Fig. 1 and 2) and that profound changes occurred during the transition from a planktonic (free-swimming) organism to one that became part of a complex, surface-attached community. While such observations have been made for several biofilm-forming microorganisms (19, 56, 65), information is lacking regarding the phenotypic characterization of the *S. pneumoniae* biofilm developmental process.

To determine whether the development of biofilms correlated with extensive proteomic changes, we elected to make use of a 2D gel-based approach, followed by protein identification via MALDI-TOF mass spectrometry by peptide mass fingerprinting. To investigate the degree to which biofilm stage-specific physiologies differ in the biofilm developmental process, crude protein extracts from planktonic cells and three biofilm developmental stages were prepared and analyzed by 2D-PAGE. Initially, we determined the best first-dimensional separation protocol. As shown in Fig. 4A, *S. pneumoniae* serotype 3 proteins obtained from 6-day-old biofilm cells were detectable over a wide pH range (pH 3 to 10NL), but the majority clustered within the acidic pH range, as indicated by the high abundance of protein spots on the left side of the 2D image. We therefore separated the protein extracts using a pH range of 4 to 7 (Fig. 4B), from which an average of 700 proteins was detectable. This number increased to 1,100 when proteins were separated using a pH range of 4.5 to 5.5 (Fig. 4C), which also provided greater spot resolution. Similar results were obtained for *S. pneumoniae* proteins obtained from planktonic cells (data not shown). Since the majority of the protein spots (~80 to 90%) were detectable in this narrow pH range (Fig. 4C), we used this procedure for all subsequent analyses.

S. pneumoniae serotype 3 cells were harvested after 3, 6, and 9 days of biofilm growth and from planktonic cells grown to exponential phase. The 2D images from these four conditions were compared and analyzed using Image Master 2D Platinum software. Representative examples of 2D protein patterns of the three biofilm developmental stages and the planktonic growth stage are shown in Fig. 5. Comparison of protein patterns of planktonic and biofilm cells after various attachment times revealed differential protein production depending on the stage of biofilm development.

When the protein patterns of planktonic cells were compared to the patterns of 3-day-old biofilms, more than 30% of the detectable proteome was found to be different; 14% of the detectable proteome was found to be upregulated and 18% downregulated. In addition, approximately 200 proteins were synthesized de novo. A similar degree of difference was found between the protein patterns of 6- and 9-day-old biofilms. Between 6 and 9 days of biofilm formation, more than 40% of the proteome was found to be differentially produced; ~20%

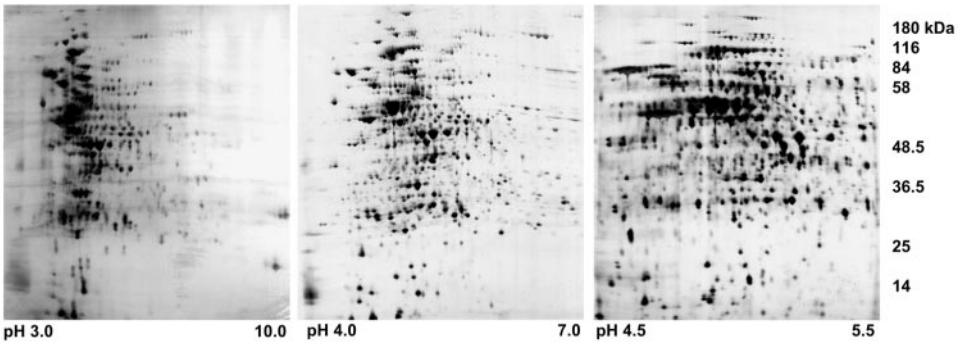

FIG. 4. 2D images of total cell extracts obtained from 6-day-old *Streptococcus pneumoniae* capsule serotype 3 biofilms. The total protein extracts (200 μg) were separated using (A) pH 3 to 10NL, (B) pH 4 to 7 and (C) pH 4.5 to 5.5 Immobiline Dry Strips in the first dimension, followed by SDS-PAGE using 11% polyacrylamide gels in the second dimension. Gels were stained with silver nitrate (10).

of all detectable proteins were found to be more expressed and 21% of the proteome were less expressed after 9 days of biofilm growth. Furthermore, approximately 60 proteins were synthesized de novo.

The smallest difference was detected between the protein profiles of 3- and 6-day-old biofilms. This transition was correlated with an approximately 20% change in the protein profile. Only 12% of the detectable proteome was upregulated and less than 8% was downregulated. However, the transition between 6 and 9 days of biofilm formation was accompanied with the de novo production of more than 250 proteins. Interestingly, when the protein patterns of 9-day-old biofilms were compared to the patterns of planktonic cells, more than 11% of the detectable proteome was upregulated and 34% was downregulated, indicating that over the biofilm developmental life cycle of *S. pneumoniae*, only ~54% of all the proteins were produced constantly.

Over the course of biofilm development, the number of detectable 2D protein spots increased from approximately 400 under planktonic growth conditions to more than 1,200 under

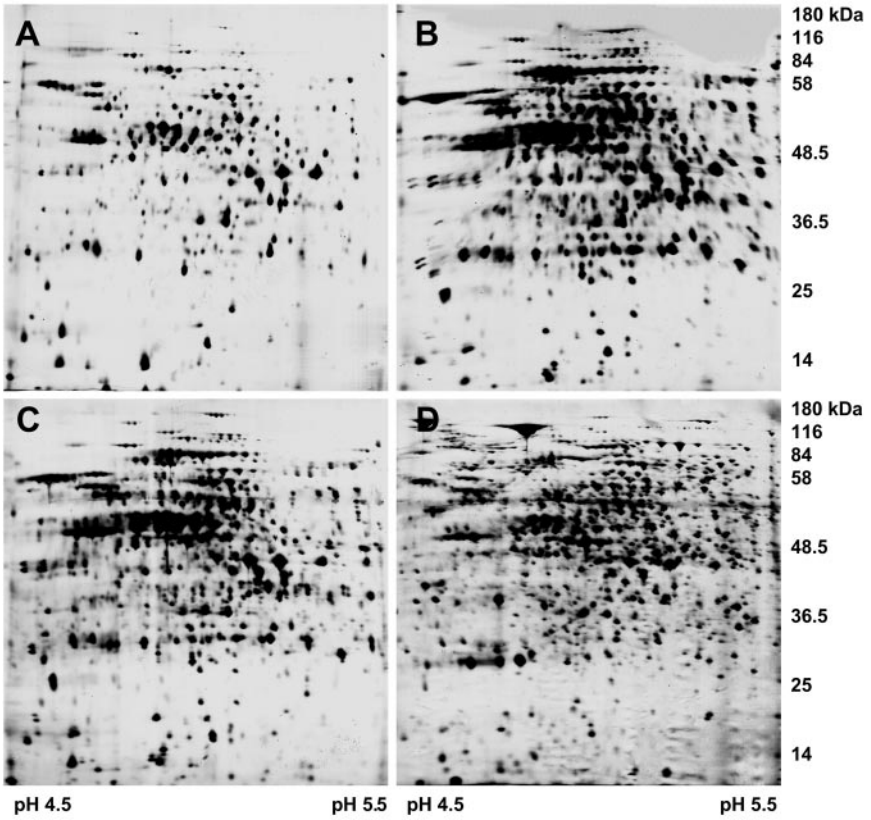

FIG. 5. 2D images of total cell extracts obtained from *Streptococcus pneumoniae* serotype 3 grown planktonically (A) and as 3-day (B), 6-day (C), and 9-day (D) biofilm. The crude protein extracts (200 μg) were separated on pH 4.5 to 5.5 Immobiline Dry strips, followed by SDS-PAGE using 11% polyacrylamide gels. Gels were stained with silver nitrate (10). Experiments were performed in triplicate.

TABLE 4. Average number of spots and average total protein spot volume per 2D image[a]

Growth conditions	No. of spots per 2D image	Overall spot volume per 2D image
Planktonic	452 (89)	1,080 (14)
3-day-old biofilm	763 (33)	2,925 (202)
6-day-old biofilm	1,100 (6)	2,152 (472)
9-day-old biofilm	1,167 (24)	2,459 (133)

[a] 2D images obtained from *S. pneumoniae* serotype 3 grown planktonically and after 3, 6, and 9 days of biofilm growth were analyzed using the Image Master 2D Platinum software (GE Healthcare). Experiments were carried out in triplicate for each growth stage. Numbers in parentheses are standard deviations.

9-day biofilm growth conditions (Table 4). Recently, the genomes of two *S. pneumoniae* strains, R6 and TIGR4, have been sequenced and annotated (36, 68). Depending on the pneumococcal strain, between 2,000 and 2,200 predicted protein-coding regions have been identified. Thus, our data indicate that under planktonic growth conditions, approximately 20% of all predicted protein coding regions were detectable within the pH 4.5 to 5.5 range. However, upon biofilm formation (9-day-old biofilm), more than 50% of all predicted protein-coding genes were detectable within this range (Fig. 5 and Table 4). Thus, on average, more than 700 2D protein spots (~30% of all predicted protein-coding genes) that were detectable in the protein patterns of mature 9-day-old biofilms were absent in planktonic cells. The increase in spot number was accompanied by an increase in the overall spot intensity. Within 9 days of biofilm growth, the spot intensity increased from approximately 1,000 under planktonic growth conditions to 2,450 under mature biofilm growth conditions (Table 4).

Difference in protein production patterns over the course of *Streptococcus pneumoniae* biofilm development is not a result of varied protein loads. To demonstrate that the differences in the protein profiles are a result of bacteria adapting to life at a surface, and not the result of various protein loads per 2D image, we separated the total protein extracts (5 μg) obtained from all four growth conditions by sodium dodecyl sulfate (SDS)-PAGE and subsequently stained the SDS gel with silver nitrate (data not shown). The four samples showed similar staining intensity. This was confirmed by image analysis indicating that equal protein amounts were separated on the one-dimensional SDS gel. Furthermore, we excluded the possibility of the protein production patterns being a result of differences in cell numbers, as the CFU number was closely correlated with the total protein recovered for all three biofilm developmental stages, as 10^8 CFU always yielded ~1 μg of protein. As a result, the differences in protein spot volume and the number of protein spots per 2D image are most likely attributable to the selection of a narrow pH range (pH 4.5 to 5.5), which resulted in the loss of proteins outside this range (pH 5.5 to 10; Fig. 4). This finding also points toward potential proteomic changes in the pH 5.5 to 10 range.

Identification of proteins that were differentially produced over the course of biofilm development. Several proteins that were differentially produced over the course of biofilm development were identified by MALDI-TOF mass spectrometry using peptide mass fingerprinting (Table 5). The proteins have been characterized according to function and represent several different categories, including metabolism/biosynthesis, capsule production, virulence, surface-associated proteins, and others.

Proteins that were grouped in the metabolism/biosynthesis category carbon metabolism have been identified as NADP-specific glutamate dehydrogenase, aminopeptidase N, dihydroorotate dehydrogenase, inosine-5-monophosphate dehydrogenase, glutamine aminotransferase, glycosylhydrolase family I, phosphoglyceromutase, and phosphoenolpyruvate carboxylase. Proteins in this category were found to be more abundant under biofilm growth conditions with the exception of NADP-specific glutamate dehydrogenase (Table 5). Similarly, glucose-6-phosphate isomerase and phosphoglycerate kinase were found to be most abundant under planktonic growth conditions (Table 5 and Fig. 6A). Interestingly, all three enzymes have been shown to be involved in glycolysis, gluconeogenesis, and starch metabolism. The other two proteins identified involved in energy metabolism, ATP synthetase F1 and the fructose-stimulated pyruvate kinase, were found to be produced at higher concentrations under biofilm growth conditions compared to planktonic growth conditions.

Proteins involved in translation or processing have been identified as 30S and 50S ribosomal proteins, exodeoxyribonuclease, peptide chain release factor 3, and elongation factors (G, P, and Tu family proteins) (Table 5). Although the concentrations of these proteins were found to be more abundant under biofilm growth conditions, their protein production profile followed the patterns shown in Fig. 6B. We identified only one protein involved in capsule production as UDP-glucose dehydrogenase. Several surface-associated proteins were identified, including enolase, peptide methionine sulfoxide reductase (MsrA), and glyceraldehyde-3-phosphate dehydrogenase (Table 5). The production patterns of all identified surface-associated proteins followed the one shown in Fig. 6C. Additionally, two proteins associated with virulence were identified as pneumolysin and pyruvate oxidase. Both proteins were found to be most abundant under biofilm growth conditions, and their production pattern followed the pattern shown in Fig. 6C.

DISCUSSION

Previous biofilm culture techniques have not provided a detailed phenotypic characterization of the biofilm developmental process by *Streptococcus pneumoniae*. Here, we describe a continuous-flow biofilm reactor system that allowed us to cultivate and phenotypically characterize biofilm formation by *S. pneumoniae*. Microscopic methods were used to illustrate biofilm development and to visualize the overall biofilm architecture. By doing so, we determined that biofilm formation in *S. pneumoniae* occurred in stages: in the first stage (day 1), individual planktonic cells were observed to attach to the surface, and in the second stage (days 2 to 3), cellular aggregates formed, presumably via replication of the initially attached cells (Fig. 1). By day 6, microcolony formation was observable for some strains wherein the biofilms had fully developed, and attained maximum cell density (biomass) and height (Fig. 2 and 3). Biofilm development has been shown in many bacterial species to progress through multiple developmental stages (19, 20, 55, 58, 71). The developmental process for *S. pneumoniae* observed in this study is similar to that of *P. aeruginosa*, for

TABLE 5. Proteins produced[a]

Group and function	Protein	Gene	Stage of maximum production	Molecular mass (kDa)	pI	No. of matched peptides
Metabolism/biosynthesis						
Carbon metabolism	NADP-specific glutamate dehydrogenase	*gdhA* (spr1181)	Planktonic growth	48.95	5.4	6/6
	Aminopeptidase N	*pepN* (spr0706)	Day 3	95.45	4.8	4/4
	Thiamine biosynthesis lipoprotein	*apbE* (spr1324)	Day 3	33.9	5	4/4
	Inosine-5′-monophosphate dehydrogenase	*imdH* (spr2033)	Day 3	52.54	5.2	4/4
	Glutamine aminotransferase	SP0266	Day 3	57.68	4.9	4/4
	Dihydroorotate dehydrogenase	*pyrDA* (spr0672)	Day 3	34.79	5	2/2
	Phosphoenolpyruvate carboxylase	*ppc* (spr0974)	Day 3	103.48	5.5	5/5
	Phosphoglyceromutase	*gpmA* (spr1499)	Day 3	26.03	5.1	3/3
	L-Lactate dehydrogenase	*ldh* (spr1100)	Day 3	35.06	5	4/4
Energy metabolism	Glucose-6-phosphate isomerase	*gpi* (spr1882)	Planktonic growth	49.85	5	5/10
	Phosphoglycerate kinase	*pgk* (spr0441)	Planktonic growth	41.92	4.9	4/4
	Glycosylhydrolase family I	SP0265	Day 3	53.23	5.1	3/3
	Pyruvate kinase I; fructose-stimulated	*pykF* (spr0797)	Day 3	54.79	5.0	4/4
	Proton-translocating ATPase F1 sector; alpha subunit	*atpA* (spr1362)	Day 3	54.68	5	4/8
Nucleotide metabolism	Ribonucleoside disphosphate reductase (major subunit)	*nrdE* (spr1065)	Day 3	81.86	5.3	9/9
	Alanyl-tRNA synthetase	*alaS* (spr1240)	Day 3	96.56	5	6/6
	Purine nucleoside phosphorylase	*pnp* (spr0734)	Day 3	29	5.2	5/5
	Histidyl-tRNA synthetase	*hisS* (spr1931)	Day 3	48.75	5.2	5/5
	Glutamine amidotransferase	*gauA* (spr1300)	Day 3	57.68	4.9	5/5
	Lysyl-tRNA synthetase	*lysS* (spr0626)	Day 3	56.15	5.3	3/3
	Glycyl-tRNA synthetase beta chain	*glyS* (spr1328)	Day 9	75.54	4.9	3/3
Lipid biosynthesis	Acetyl-coenzyme A carboxylase, biotin carboxylase	accC (spr0385)	Day 3	49.81	5.1	4/4
	Glycerol-3-phosphate dehydrogenase $(NADP)^+$	*gpdA* (spr1902)	Day 3	36.76	5.2	4/4
Translation/processing	30S ribosomal protein S1	*rpsA* (spr0764)	Day 3	43.86	5.1	11/11
	Peptide chain relase factor 3	*prfC* (spr0396)	Day 3	58.47	5.1	4/7
	30S ribosomal protein S2	*rpsB* (spr2020)	Day 3	28.85	5.1	11/11
	Translation elongation factor Tu	*tufA* (spr1343)	Day 3	43.96	4.8	12/15
	50S ribosomal protein L10	*rplJ* (spr1212)	Day 3	17.46	5.1	2/2
	Exodeoxyribonuclease	*exoA* (spr1660)	Day 3	31.05	5.2	4/4
	Elongation factor Tu family	SP0681	Day 6	68.24	4.8	5/5
	Elongation factor G	*fusA* (spr0250)	Day 6	76.87	4.9	3/3
	Elongation factor P	*efp* (spr0392)	Day 9	20.58	4.9	3/3
Capsule production	UDP-glucose dehydrogenase	*ugd* (spr0139)	Day 3	44.83	5	5/5
Surface-associated proteins	Glyceraldehyde-3-phosphate dehydrogenase	SP2012	Day 3	35.95	5.3	8/8
	Peptide methionine sulfoxide reductase	*msrA* (spr1217)	Day 3	35.91	4.9	5/5
	Enolase	*eno* (spr1036)	Day 3	47.14	4.7	11/14
	DnaK protein	*dnaK* (spr0455)	Day 3	64.82	4.6	5/8
Virulence	Pyruvate oxidase	*spxB* (spr0642)	Day 6	65.36	5.1	10/15
	Pneumolysin	*ply* (spr1739)	Day 3	52.94	5.1	8/11
Other	Hypothetical protein, interruption	SP0329	Day 3	12.96	5.1	3/3
	Conserved hypothetical protein		Day 3	21.08	5.1	3/3
	Cof family protein/peptidyl-prolyl *cis-trans* isomerase, cyclophilin type	SP1538	Day 9	52.05	4.8	4/4

[a] The production pattern analysis was carried out from 2D images that were scanned using a calibrated image scanner (GE Healthcare). Image analysis was done using the Image Master 2D Platinum software (GE Healthcare). Computational analysis was based on 2D protein spot volume. Proteins were identified by tryptic in-gel digestion followed by peptide mass fingerprinting as described in Materials and Methods using the annotated genomes of *S. pneumoniae* TIGR4 and R6. All proteins listed here were identified with significant certainty (probability score of <0.03). Proteins were identified with 3 to 12 matched peptides and a minimum of 10% sequence coverage.

which five stages can be distinguished (55, 65), however, as yet, we have not observed biofilm dispersion.

Biofilm development by *S. pneumoniae* was accompanied by extensive changes at the protein level, with differences in the concentration of the proteins ranging from 20 to 40% among the four growth stages examined. The greatest degree of difference among the four protein profiles was evidenced by the protein profiles of planktonic and 9-day biofilm cells (Fig. 5). More than 45% of all detectable proteins were differentially produced over the course of biofilm development (Fig. 5). The increase in the number of detectable proteins may be best explained by protein modification, changes in the growth conditions, and/or adaptation to the sessile mode of growth. Environmental factors such as iron, oxygen, and lack of carbon sources have been shown not only to influence protein production within biofilms but also to profoundly impact biofilm formation by *P. aeruginosa* and other biofilm-forming bacteria (1, 11, 37, 62, 69, 72).

Here, we demonstrated that metabolic proteins and housekeeping proteins were differentially produced over the course of biofilm development (Table 5). Our findings are consistent with previous studies indicating that microorganisms undergo profound metabolic and phenotypic changes during their transition from planktonic (free-swimming) organisms to complex, highly developed surface-attached biofilm communities (18–19, 21, 47, 52, 54–55, 65). However, none of the previous studies indicated a dramatic increase in the number of detectable protein spots as found in this study (Fig. 5 and Table 4). Here, biofilm formation was coincident with de novo protein production. More than 700 2D protein spots that were detectable in the protein patterns of mature 9-day-old biofilms were absent in planktonic cells (Table 4), indicating that biofilm

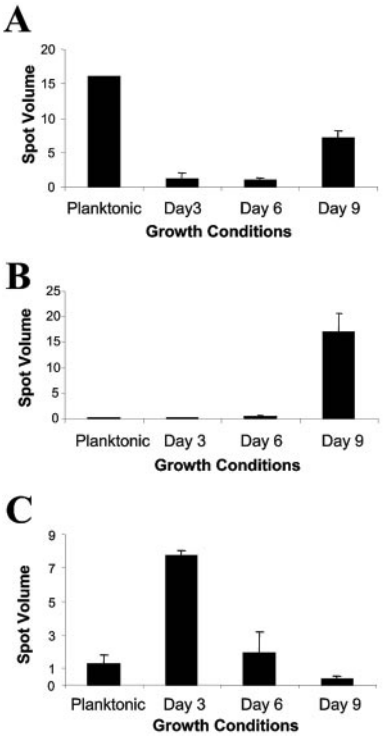

FIG. 6. Protein production patterns of selected proteins over the course of *Streptococcus pneumoniae* serotype 3 biofilm development. Representative production patterns of glucose-6-phosphate isomerase (A), glycl-tRNA synthetase (B), and pneumolysin (C). The production pattern analysis was carried out from 2D images that were scanned using a calibrated image scanner (GE Healthcare). Image analysis was done using the Image Master 2D Platinum software (GE Healthcare). Computational analysis was based on 2D protein spot volume. The planktonic growth stage and three biofilm developmental stages were analyzed thus: planktonic, planktonic cell stage; 3 days, 3-day-old biofilms; 6 days, 6-day-old biofilms, and 9 days, 9-day-old biofilms. The data shown here represent the average spot volumes. Experiments were carried out in triplicate for each growth stage.

formation correlated with the de novo synthesis by ~30% of all predicted protein-coding genes.

Furthermore, we noted an increased abundance of proteins involved in resistance and virulence, including pneumolysin, methionine sulfoxide reductase, pyruvate oxidase, and UDP-glucose dehydrogenase, in *S. pneumoniae* biofilms compared to their planktonic counterparts. Pneumolysin is a toxin involved in lysing cholesterol-containing membranes (53) by forming pores in eukaryotic cell membranes, while pyruvate oxidase was shown to contribute to resistance to hydrogen peroxide (48, 64) and to cytotoxic effects on host cells and tissues (50). In *S. pneumoniae* type 3, capsule production relies on the activity of UDP-glucose dehydrogenase (2). Early work has shown that the amount of capsular polysaccharide of some pneumococci (e.g., serotype 3) directly correlates to increased virulence (41, 44) and resistance to phagocytosis (59).

Recently, a role for the capsule in colonization has been described (45). Using isolates containing defined mutations in the capsule locus, these authors demonstrated that expression of the capsular polysaccharide is essential for colonization by pneumococcal serotypes 2 and 3. Nonencapsulated derivatives of each of these strains were unable to colonize BALB/cByJ mice, while mutant strains producing approximately 20% of the parental amount of capsule colonized as effectively as the parent (45). Our finding of increased production of UDP-glucose dehydrogenase (which is involved in capsule production) is consistent with the role of the capsule in virulence and attachment.

Several additional proteins were identified that have been previously implicated in attachment, including enolase and glyceraldehyde-3-phosphate dehydrogenase (6–7, 28, 49). Overall, our findings indicate that biofilm development in *S. pneumoniae* is correlated with profound phenotypic changes and that *S. pneumoniae* biofilms produce proteins associated with attachment, bacterial resistance, and virulence at a higher level than their planktonic counterparts, a characteristic that has been well known of biofilms formed by other species (8, 16, 22, 32, 72).

Another characteristic of biofilms is their architecture. Three major architectural groups were evident, depending upon the particular clinical strain used in the study (Fig. 3 and Table 3). Group I biofilms formed distinct microcolonies and pronounced water channels, whereas group II biofilms, although relatively similar in thickness, appeared to be less structured, lacking large microcolonies and pronounced water channels. The group III biofilms were discernible as flat structures composed only of very small cell clusters (Fig. 3 and Table 3). Whether the genetic background, the capsular type, or both determine the overall biofilm architecture is unclear.

Studies of two completed *S. pneumoniae* genome sequences have indicated substantial diversity between strains and serotypes (36, 68). However, the finding of distinct biofilm architectural groups (depending upon the particular clinical strain) may be important in pneumococcal diseases. Some capsular serotypes have been shown to cause more severe and lethal disease than others (12). Mortality rates from invasive disease were increased with serotypes 3, 5, and 23, while infections with serotypes 1, 4, 6, 9V, 12F, and 14 were associated with lower mortality rates (3, 31, 34, 46). Furthermore, during experimental pneumococcal meningitis serotypes 3 and 23 caused more severe inflammation than serotypes 1, 5, 9, and 7F (26, 67). Interestingly, serotypes 3 and 23 were categorized here as group I biofilms and serotypes 6, 9, and 14 as group II biofilms (Fig. 3 and Table 3).

In conclusion, we have demonstrated that the continuous-culture biofilm system is suitable for cultivating and characterizing biofilm formation by *S. pneumoniae* strains of various genetic backgrounds and capsular types. The biofilm reactor provided a means for visualizing, quantifying, and collecting biofilm-associated cells over time. We also demonstrated that the biofilm developmental process in *S. pneumoniae* occurs in stages which are accompanied by large-scale changes at the protein level. Furthermore, biofilm development was accompanied by an increased production of several proteins involved in attachment, resistance, and virulence. The data provided here may provide a link between the formation and the architecture of biofilms and pneumococcal diseases. However, whether the genetic background, the capsular type, or both affect the overall biofilm architecture and/or virulence is currently being further investigated.

ACKNOWLEDGMENTS

We thank David Greenberg for providing pneumococcal strains. We thank Luanne Hall-Stoodley for valuable discussions.

This work was supported by grants from the National Institutes of Health (RO1 DC005659) and the National Science Foundation (DBI-0321046 and 0311307).

REFERENCES

1. **Applegate, D. H., and J. D. Bryers.** 1991. Effects on carbon and oxygen limitations and calcium concentrations on biofilm removal processes. Biotechnol. Bioeng. **37:**17–25.
2. **Arrecubieta, C., R. Lopez, and E. Garcia.** 1994. Molecular Characterization of *cap3A*, a gene from the operon required for the synthesis of the capsule of *Streptococcus pneumoniae* type 3: sequencing of mutations responsible for the unencapsulated phenotype and localization of the capsular cluster on the pneumococcal chromosome. J. Bacteriol. **176:**6375–6383.
3. **Austrian, R., and J. Gold.** 1964. Pneumococcal bacteremia with especial reference to bacteremic pneumococcal pneumonia. Ann. Intern. Med. **60:** 759–776.
4. **Balachandran, P., S. K. Hollingshead, J. C. Paton, and D. E. Briles.** 2001. The autolytic enzyme LytA of *Streptococcus pneumoniae* is not responsible for releasing pneumolysin. J. Bacteriol. **183:**3108–3116.
5. **Bennett, K. E., M. P. Haggard, P. A. Silva, and I. A. Stewart.** 2001. Behaviour and developmental effects of otitis media with effusion into the teens. Arch. Dis. Child. **85:**91–95.
6. **Bergmann, S., M. Rohde, and S. Hammerschmidt.** 2004. Glyceraldehyde-3-phosphate dehydrogenase of *Streptococcus pneumoniae* is a surface-displayed plasminogen-binding protein. Infect. Immun. **72:**2416–2419.
7. **Bergmann, S., M. Rohde, G. S. Chhatwal, and S. Hammerschmidt.** 2001. α-Enolase of *Streptococcus pneumoniae* is a plasmin(ogen)-binding protein displayed on the bacterial cell surface. Mol. Microbiol. 2001. **40:**1273–1287.
8. **Bjarnsholt, T., P. O. Jensen, M. Burmolle, M. Hentzer, J. A. Haagensen, H. P. Hougen, H. Calum, K. G. Madsen, C. Moser, S. Molin, N. Hoiby, and M. Givskov.** 2005. *Pseudomonas aeruginosa* tolerance to tobramycin, hydrogen peroxide and polymorphonuclear leukocytes is quorum-sensing dependent. Microbiology **151:**373–383.
9. **Bluestone, C. D., J. S. Stephenson, and L. M. Martin.** 1992. Ten-year review of otitis media. Pediatr. Infect. Dis. J. **11:**S7–S11.
10. **Blum, H., H. Beier, and H. J. Gross.** 1987. Improved silver staining of plant proteins, RNA and DNA in polyacrylamide gels. Electrophoresis **8:**93–99.
11. **Bollinger, N., D. J. Hassett, B. H. Iglewski, J. W. Costerton, and T. R. McDermott.** 2001. Gene expression in *Pseudomonas aeruginosa*: evidence of iron override effects on quorum sensing and biofilm-specific gene regulation. J. Bacteriol. **183:**1990–1996.
12. **Briles, D. E., M. J. Crain, B. M. Gray, C. Forman, and J. Yother.** 1992. Strong association between capsular type and virulence for mice among human isolates of *Streptococcus pneumoniae*. Infect. Immun. **60:**111–116.
13. **Budhani, R. K., and J. K. Struthers.** 1997. The use of Sorbarod biofilms to determine the antimicrobial susceptibilities of a strain of *Streptococcus pneumoniae*. J. Antimicrob. Chemother. **40:**601–602.
14. **Costerton, J. W., Z. Lewandowski, D. DeBeer, D. Caldwell, D. Korber, and G. James.** 1994. Biofilms, the customized microniche. J. Bacteriol. **176:**2137–2142.
15. **Costerton, J. W., Z. Lewandowski, D. Caldwell, D. Korber, and H. M. Lappin-Scott.** 1995. Microbial biofilms. Annu. Rev. Microbiol. **49:**711–745.
16. **Costerton, J. W., P. S. Stewart, and E. P. Greenberg.** 1999. Bacterial biofilms: a common cause of persistent infections. Science **284:**1318–1322.
17. **Costerton, W., R. Veeh, M. Shirtliff, M. Pasmore, J. C. Post, and G. D. Ehrlich.** 2003. The application of biofilm science to the study and control of chronic bacterial infections. J. Clin. Investig. **112:**1466–1477.
18. **Dagastino, L. A. E. Goodman, and K. C. Marshall.** 1991. Physiological responses induced in bacteria adhering to surfaces. Biofouling **4:**113–119.
19. **Davey, M. E., and G. A. O'Toole.** 2000. Microbial biofilms: from ecology to molecular genetics. Microbiol. Mol. Biol. Rev. **64:**847–867.
20. **Davies, D. G., and G. G. Geesey.** 1995. Regulation of the alginate biosynthesis gene *algC* in *Pseudomonas aeruginosa* during biofilm development in continuous culture. Appl. Environ. Microbiol. **61:**860–867.
21. **Davies, D. G., and G. A. McFeters.** 1988. Growth and comparative physiology of *Klebsiella oxytoca* attached to granular activated carbon particles and in liquid media. Microb. Ecol. **15:**165–175.
22. **Donlan, R. M., and J. W. Costerton.** 2002. Biofilms: survival mechanisms of clinically relevant microorganisms. Clin. Microbiol. Rev. **15:**167–193.
23. **Donlan, R. M., J. A. Piede, C. D. Heyes, L. Sanii, R. Murga, P. Edmonds, I. El-Sayed, and M. A. El-Sayed.** 2004. Model system for growing and quantifying *Streptococcus pneumoniae* biofilms in situ and in real time. Appl. Environ. Microbiol. **70:**4980–4988.
24. **Ehrlich, G., R. Veeh, X. Wang, J. W. Costerton, J. D. Hayes, F. Z. Hu, B. J. Daigle, M. D. Ehrlich, and J. C. Post.** 2002. Mucosal biofilm formation on middle-ear mucosa in the chinchilla model of otitis media. JAMA **287:**1710–1715.
25. **Ehrlich, G. D., Z. F. Hu, and J. C. Post.** 2004. Role for biofilms in infectious disease, p. 332–358. In M. Ghannoum and, G. A. O'Toole (ed.), Microbial biofilms. ASM Press, Washington, D.C.
26. **Engelhard, D., S. Pomeranz, R. Gallily, N. Strauss, and E. Tuomanen.** 1997. Serotype-related differences in inflammatory response to *Streptococcus pneumoniae* in experimental meningitis. J. Infect. Dis. **175:**979–982.
27. **Faden, H., L. Duffy, and M. Boeve.** 1998. Otitis media: back to the basics. Pediatr. Infect. Dis. J. **17:**1105–1113.
28. **Ge, J., D. M. Catt, and R. L. Gregory.** 2004. *Streptococcus mutans* surface α-enolase binds salivary mucin MG2 and human plasminogen. Infect. Immun. **72:**6748–6752.
29. **Geesey, G. G., W. T. Richardson, H. G. Yeomans, R. T. Irvin, and J. W. Costerton.** 1977. Microscopic examination of natural sessile bacterial populations from an alpine stream. Can. J. Microbiol. **23:**1733–1736.
30. **Giebink, G. S.** 1989. The microbiology of otitis media. Pediatr. Infect. Dis. **8:**S18–S20.
31. **Gransden, W. R., S. J. Eykyn, and I. Phillips.** 1985. Pneumococcal bacteraemia: 325 episodes diagnosed at St Thomas's Hospital. Br. Med. J. Clin. Res. **290:**505–508.
32. **Hassett, D. J., J. F. Ma, J. G. Elkins, T. R. McDermott, U. A. Ochsner, S. E. West, C. T. Huang, J. Fredericks, S. Burnett, P. S. Stewart, G. McFeters, L. Passador, amd B. H. Iglewski.** 1999. Quorum sensing in *Pseudomonas aeruginosa* controls expression of catalase and superoxide dismutase genes and mediates biofilm susceptibility to hydrogen peroxide. Mol. Microbiol. **34:** 1082–1093.
33. **Henrichsen, J.** 1995. Six newly recognized types of *Streptococcus pneumoniae*. J. Clin. Microbiol. **33:**2759–2762.
34. **Henriques, B., M. Kalin, A. Ortqvist, B. O. Liljequist, M. Almela, T. J. Marrie, M. A. Mufson, A. Torres, M. A. Woodhead, S. B. Svenson, and G. Källenius.** 2000. Molecular epidemiology of *Streptococcus pneumoniae* causing invasive disease in 5 countries. J. Infect. Dis. **182:**833–839.
35. **Heydorn, A., B. K. Ersboll, M. Hentzer, M. R. Parsek, M. Givskov, and S. Molin.** 2000. Experimental reproducibility in flow-chamber biofilms. Microbiology **146:**2409–2415.
36. **Hoskins, J., W. E. Alborn Jr., J. Arnold, L. C. Blaszczak, S. Burgett, B. S. DeHoff, S. T. Estrem, L. Fritz, D.-J. Fu, W. Fuller, C. Geringer, R. Gilmour, J. S. Glass, H. Khoja, A. R. Kraft, R. E. Lagace, D. J. LeBlanc, L. N. Lee, E. J. Lefkowitz, J. Lu, P. Matsushima, S. M. McAhren, M. McHenney, K. McLeaster, C. W. Mundy, T. I. Nicas, F. H. Norris, M. O'Gara, R. B. Peery, G. T. Robertson, P. Rockey, P.-M. Sun, M. E. Winkler, Y. Yang, M. Young-Bellido, G. Zhao, C. A. Zook, R. H. Baltz, S. R. Jaskunas, P. R. Rosteck Jr., P. L. Skatrud, and J. I. Glass.** 2001. Genome of the bacterium *Streptococcus pneumoniae* strain R6. J. Bacteriol. **183:**5709–5717.
37. **James, G. A., D. R. Korber, D. E. Caldwell, and J. W. Costerton.** 1995. Digital image analysis of growth and starvation responses of a surface-colonizing *Acinetobacter* sp. J. Bacteriol. **177:**907–915.
38. **Kaplan, B., T. L. Wandstrat, and J. R. Cunningham.** 1997. Overall cost in treatment of otitis media. Pediatr. Infect. Dis. J. **16:**S9–S11.
39. **Kerr, C. J., Osborn, K. S., Rickard, A. H., Robson, G. D., and Handley, P. S.** 2003. Biofilms in water distribution systems, p. 757–776. *In* M. Duncan and N. J. Horan (ed.)., Water and wastewater engineering. Academic Press, London, United Kingdom.
40. **Khoury, A. E., K. Lam, B. Ellis, and J. W. Costerton.** 1992. Prevention and control of bacterial infections associated with medical devices. ASAIO J. **38:**M174–178.
41. **Kim, J. O., and J. N. Weiser.** 1998. Association of intrastrain phase variation in quantity of capsular polysaccharide and teichoic acid with the virulence of *Streptococcus pneumoniae*. J. Infect. Dis. **177:**368–377.
42. **Klein, D. L.** 1999. Pneumococcal disease and the role of conjugate vaccines. Microb. Drug Resist. **5:**147–157.
43. **Lamont, R. J., and H. F. Jenkinson.** 1998. Life below the gum line: pathogenic mechanisms of Porphyromonas gingivalis. Microbiol. Mol. Biol. Rev. **62:**1244–1263.
44. **MacLeod, C. M., and M. R. Krauss.** 1950. Relation of virulence of pneumococcal strains for mice to the quantity of capsular polysaccharide formed *in vitro*. J. Exp. Med. **92:**1–9.
45. **Magee, A. D., and J. Yother.** 2001. Requirement for capsule in colonization by *Streptococcus pneumoniae*. Infect. Immun. **69:**3755–3761.
46. **Mufson, M. A., D. M. Kruss, R. E. Wasil, and W. I. Metzger.** 1974. Capsular types and outcome of bacteremic pneumococcal disease in the antibiotic era. Arch. Intern. Med. **134:**505–510.
47. **O'Toole, G. A., H. B. Kaplan, and R. Kolter.** 2000. Biofilm formation as microbial development. Annu. Rev. Microbiol. **54:**49–79.
48. **Overweg, K. A., C. D. Pericone, G. G. C. Verhoef, J. N. Weiser, H. D. Meiring, A. P. J. M. de Jong, R. de Groot, and P. W. M. Hermans.** 2000. Differential protein expression in phenotypic variants of *Streptococcus pneumoniae*. Infect. Immun. **68:**4604–4610.
49. **Pancholi, V., and V. A. Fischetti.** 1992. A major surface protein on group A streptococci is a glyceraldehyde-3-phosphate-dehydrogenase with multiple binding activity. J. Exp. Med. **176:**415–426.
50. **Pericone, C. D., K. Overweg, P. W. Hermans, and J. N. Weiser.** 2000. Inhibitory and bactericidal effects of hydrogen peroxide production by *Strep-*

tococcus pneumoniae on other inhabitants of the upper respiratory tract. Infect. Immun. **68:**3990–3997.
51. **Peterson, G. L.** 1977. A simplification of the protein assay method of Lowry et al. which is more generally applicable. Anal. Biochem. **83:**346–356.
52. **Prigent-Combaret, C., O. Vidal, C. Dorel, and P. Lejeune.** 1999. Abiotic surface sensing and biofilm-dependent regulation of gene expression in *Escherichia coli*. J. Bacteriol. **181:**5993–6002.
53. **Rubins, J. B., A. H. Paddock, D. Charboneau, A. M. Berry, J. C. Paton, and E. N. Janoff.** 1998. Pneumolysin in pneumococcal adherence and colonization. Microb. Pathog. **25:**337–342.
54. **Sauer, K., and A. K. Camper.** 2001. Characterization of phenotypic changes in *Pseudomonas putida* in response to surface-associated growth. J. Bacteriol. **183:**6579–6589.
55. **Sauer, K., A. K. Camper, G. D. Ehrlich, J. W. Costerton, and D. G. Davies.** 2002. *Pseudomonas aeruginosa* displays multiple phenotypes as a biofilm. J. Bacteriol. **184:**1140–1154.
56. **Sauer, K.** 2003. The genomics and proteomics of biofilm formation. Genome Biol. **4:**219.0–219.5.
57. **Sauer, K., M. C. Cullen, A. H. Rickard, L. A. Zeef, D. G. Davies, and P. Gilbert.** 2004. Characterization of nutrient-induced dispersion in *Pseudomonas aeruginosa* PAO1 biofilm. J. Bacteriol. **186:**7312–7326.
58. **Schembri, M. A., K. Kjaergaard, and P. Klemm.** 2003. Global gene expression in *Escherichia coli* biofilms. Mol. Microbiol. **48:**253–627.
59. **Scott, J. A., A. J. Hall, R. Dagan, J. M. Dixon, S. J. Eykyn, A. Fenoll, M. Hortal, L. P. Jette, J. H. Jorgensen, F. Lamothe, C. Latorre, J. T. Macfarlane, D. M. Shlaes, L. E. Smart, and A. Taunay.** 1996. Serogroup-specific epidemiology of *Streptococcus pneumoniae*: associations with age, sex, and geography in 7,000 episodes of invasive disease. Clin. Infect. Dis. **22:**973–981.
60. **Shen, K., J. Gladitz, P. Antalis, B. Dice, B. Janto, R. Keefe, J. Hayes, A. Ahmed, R. Dopico, N. Ehrlich, J. Jocz, J. Kropp, S. Yu, L. Nistico, D. P. Greenberg, K. Barbadora, J. C. Post, G. D. Ehrlich, and F. Z. Hu.** 2006. Characterization, distribution, and expression of novel genes among eight clinical isolates of *Streptococcus pneumoniae*. Infect. Immun. **74:**321–330.
61. **Singh, P. K., A. L. Schaefer, M. R. Parsek, T. O. Moninger, M. J. Welsh, and E. P. Greenberg.** 2000. Quorum-sensing signals indicate that cystic fibrosis lungs are infected with bacterial biofilms. Nature **407:**762–764.
62. **Singh, P. K., M. R. Parsek, E. P. Greenberg, and M. J. Welsh.** 2002. A component of innate immunity prevents bacterial biofilm development. Nature **417:**552–555.
63. **Southey-Pillig, C. J., D. G. Davies, and K. Sauer.** 2005. Characterization of biofilm-specific protein production patterns in *Pseudomonas aeruginosa* and their influence on biofilm formation. J. Bacteriol. **187:**8114–8126.
64. **Spellerberg, B., D. R. Cundell, J. Sandros, B. J. Pearce, I. Idanpaan-Heikkila, C. Rosenow, and H. R. Masure.** 1996. Pyruvate oxidase, as a determinant of virulence in *Streptococcus pneumoniae*. Mol. Microbiol. **19:**803–813.
65. **Stoodley, P., K. Sauer, D. G. Davies, and J. W. Costerton.** 2002. Biofilms as complex differentiated communities. Annu. Rev. Microbiol. **56:**187–209.
66. **Stool, S. E., and M. J. Field.** 1989. The impact of otitis media. Pediatr. Infect. Dis. J. **8:**S11–S14.
67. **Tauber, M. G., M. Burroughs, U. M. Niemoller, H. Kuster, U. Borschberg, and E. Tuomanen.** 1991. Differences in pathophysiology in experimental meningitis caused by three strains of *Streptococcus pneumoniae*. J. Infect. Dis. **163:**806–811.
68. **Tettelin, H., K. E. Nelson, I. T. Paulsen, J. A. Eisen, T. D. Read, S. Peterson, J. Heidelberg, R. T. Deboy, D. H. Haft, R. J. Dodson, A. S. Durkin, M. Gwinn, J. F. Kolonay, W. C. Nelson, J. D. Peterson, L. A. Umayam, O. White, S. L. Salzberg, M. R. Lewis, D. Radune, E. Holtzapple, H. Khouri, A. M. Wolf, T. R. Utterback, C. L. Hansen, L. A. McDonald, T. V. Feldblyum, S. Angiuoli, T. Dickinson, E. K. Hickey, I. E. Holt, B. J. Loftus, F. Yang, H. O. Smith, J. C. Venter, B. A. Dougherty, D. A. Morrison, S. K. Hollingshead, and C. M. Frasier.** 2001. Complete genome sequence of a virulent isolate of *Streptococcus pneumoniae*. Science **293:**498–506.
69. **Thormann, K. M., R. M. Saville, S. Shukla, and A. M. Spormann.** 2005. Induction of rapid detachment in *Shewanella oneidensis* MR-1 biofilms. J. Bacteriol. **187:**1014–1021.
70. **Waite, R. D., J. K. Struthers, and C. G. Dowson.** 2001. Spontaneous sequence duplication within an open reading frame of the pneumococcal type 3 capsule locus causes high-frequency phase variation. Mol. Microbiol. **42:**1223–1232.
71. **Whiteley, M., M. G. Bangera, R. E. Bumgarner, M. R. Parsek, G. M. Teitzel, S. Lory, and E. P. Greenberg.** 2001. Gene expression in *Pseudomonas aeruginosa* biofilms. Nature **413:**860–864.
72. **Yoon, S. S., R. F. Hennigan, G. M. Hilliard, U. A. Ochsner, K. Parvatiyar, M. C. Kamani, H. L. Allen, T. R. DeKievit, P. R. Gardner, U. Schwab, J. J. Rowe, B. H. Iglewski, T. R. McDermott, R. P. Mason, D. J. Wozniak, R. E. Hancock, M. R. Parsek, T. L. Noah, R. C. Boucher, and D. J. Hassett.** 2002. *Pseudomonas aeruginosa* anaerobic respiration in biofilms. Relationships to cystic fibrosis pathogenesis. Dev. Cell **3:**593–603.
73. **Zhang, W., and B. T. Chait.** 2000. ProFound: an expert system for protein identification using mass spectrometric peptide mapping information. Anal. Chem. **72:**2482–2489.